Numerical Simulation of Jet Aeroacoustics from a Solid Rocket in Static-Firing Tests

*S. Tsutsumi, K. Fukuda, R. Takaki, E. Shima, K. Fujii, and K. Ui**

**Japan Aerospace Exploration Agency*

3-1-1 Yoshinodai, Sagamihara Kanawaga, 229-8510, Japan

Abstract

Acoustic field in static-firing tests of a solid motor is analyzed using an empirical method, NASA SP-8072, and numerical simulation. It is revealed from the numerical study that the Mach wave radiated from the fluctuating jet shear-layer is a dominant noise source. The numerical simulation reasonably predicts the SPLs at all measured points within the accuracy of 4 dB in OASPL. On the other hand, the empirical method overestimates the far-field SPLs located close to the jet axis by more than 10 dB. The discrepancy observed here originates in the potential-core length model and the directivity model. Especially, the directivity model has a considerable impact on the prediction accuracy.

1. Introduction

The exhaust plume from a rocket engine generates severe pressure waves. Since the pressure wave causes acoustic loading on the payload, prediction and reduction of the acoustic level around launch vehicles at lift-off is quite important design constraint taken into consideration early in the design process of the launch-pad. NASA SP-8072[1] has been employed for the prediction of acoustic environments of various launch vehicles since 1971. The NASA SP-8072 is an empirical method based on large number of flight data and results of static-firing tests. Acoustic parameters, such as source power distribution, frequency distribution, and directivity, are modeled based on the free jet characteristics. However, mechanisms of the acoustic generation are not evident, resulting in the unsatisfactory prediction accuracy. Several studies have been carried out to overcome the limitations of the NASA SP-8072. [2-8]

While, with the recent improvement of the CFD technology and computer resource, numerical simulation of acoustic radiation from rocket exhaust plumes is becoming feasible. The authors applied the CFD to reveal the generation and radiation of the pressure wave from Japanese launch vehicles, such as the H-IIA, the M-V, and advanced solid rocket.[9-11] From the result, the Mach wave radiated from the supersonic plume is found to be the major noise source. It also turns out that the shape of the deflector is very sensitive to the acoustic generation. The knowledge obtained here is used for designing the launch-pad configuration.

Table 1: Specifications of the motor.

Trust at sea level	Me	Re	Pe/Pa	To/Ta	De	M_J	D_J
260 kN	2.92	1.75×10^6	0.418	11.2	0.614 m	2.47	0.446 m

Recently, JAXA conducted static-firing tests of a solid booster to obtain acoustic data with sufficient reliability. Mechanism of the acoustic radiation is analyzed based on the numerical simulation. Then, through the comparison with the measured acoustic data, prediction accuracy of the numerical simulation and the empirical methods are evaluated. This study discusses the updated models of the empirical method proposed by the recent studies.[2,4,6-8]

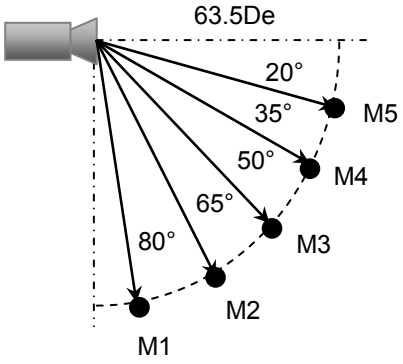

(a) Far-field.

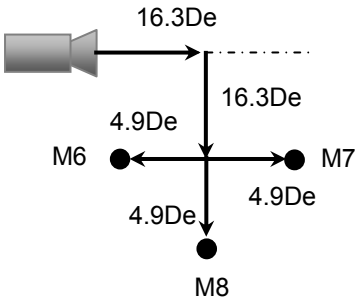

(b) Near-field.

Figure 1: Layout of microphones.

2. Outline of the Static-firing Tests

Acoustic measurements were conducted in two series of static-firing tests of a solid motor at the JAXA's Noshiro Testing Center. Motor specifications are listed in Table 1. The plume ejected from the motor is in the overexpanded condition (Pe/Pa=0.418), and the Reynolds number based on the nozzle exit condition (Re) is 1.75×10^6, which is one order of magnitude below the typical large-scale motors employed in the launch vehicles. Microphones (M1-M5) are installed at 63.5De radius at far-field arc as indicated in Fig.1(a). In addition, the near-field measurements were also conducted at 3 locations (M6-M8) as shown in Fig.1(b), since prediction of the near-field acoustic environment is inevitable in the design phase.

The static-firing tests were conducted in the test field facing the shoreline. The setups of the data acquisition systems and the evaluation of the measuring results should be carefully considered to assure the reliability. Discussion on the principal factors that influence on the reliability, such as the microphone types, the background noise, and the ground effect, are given in the reference. [12]

3. Methods of Analysis

3.1 Empirical Prediction Method

The NASA SP-8072 [1] is a de facto standard method for predicting the acoustic environment of the launch vehicle at lift-off. Acoustic source is allocated along the flow axis. There are two types of methods for the source allocation. This study focuses on the 2nd method in which the flow axis is divided into a number of regions where the total sound power and the frequency spectrum are assigned. There are mainly three parameters that are sensitive to the result: 1) acoustic efficiency, 2) potential-core length, and 3) directivity.

The overall acoustic power (W_{OA}) radiated from the rocket plume is estimated as follows:

$$W_{OA} = \eta W_M \tag{1}$$

Here, W_M represents the mechanical power of the jet (=$1/2\dot{m}V_J^2$, $\dot{m}$: mass flux, V_J: fully-expanded jet velocity), and η is the acoustic efficiency. According to the reference[1], the acoustic efficiency varies between 0.2% and 1% in many cases, but the choice of the parameter is rather arbitrary. The acoustic efficiency in this study is evaluated as 0.84 % based on Sutherland's method.[8]

Source power distribution along the jet axis is defined by the empirical curve shown in Fig.2. Denominator of the horizontal axis, Lc, represents the potential-core length. Eldred et al.[1] define the potential-core length (Lc) as follows,

$$L_c = 3.45 D_e \left(1 + 0.38 M_e\right)^2 \tag{3}$$

While, Varnier[4] recently pointed out that the Eq.3 shows disagreement with some measurements and proposed new model in which the Lc is shorter than the original one,

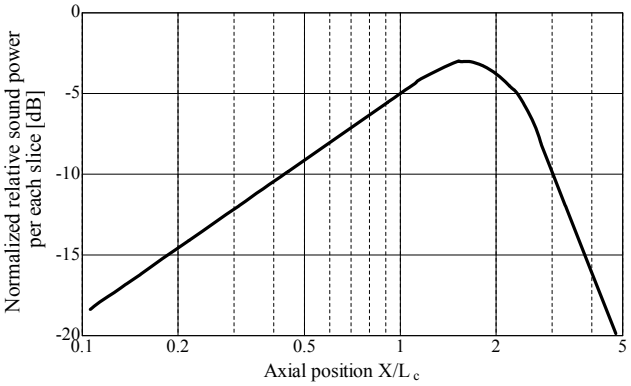

Figure 2: Source-power distribution defined in the NASA SP-8072.[1]

$$L_c = 1.75 D_J \left(1 + 0.38 M_J\right)^2 \tag{4}$$

In Eq.3, D_e and M_e represent the diameter and the Mach number at the nozzle exit. In Eq.4, on the other hand, D_J and M_J denote the Mach number and the jet diameter at fully-expanded jet condition. Those values in the current motor are also listed in Table 1. Since it is almost impossible to directly measure the potential-core length of the real rocket motor, discussions on the potential-core length modeling are still going on.[6,7,13] In the present study, these two models are examined through the comparison with the mueasuring result and the numerical result.

The directivity model, called directivity index in the NASA SP-8072, is defined as the difference between the SPL at each microphone and the value averaged over the n microphones at far-field arc,

$$\mathrm{DI}(f,\theta) = \mathrm{SPL}_{f,\theta} - 10\log\left(\frac{1}{n}\sum_{i}^{n} 10^{\mathrm{SPL}_{f,\theta}/10}\right) \quad (5)$$

Plotkin et al.[6] and Haynes et al.[7] propose their own directivity indexes based on their own measurements. To the authors' knowledge, effect of the directivity model on the prediction accuracy is not evident still now. Thus, the directivity is also discussed in the present study.

3.2 Numerical Simulation (CFD)

Recent studies on the jet aeroacoustics employ the numerical techniques with higher-order schemes both for the spatial and temporal discretization.[14] Our aim is to design the launch-pad with lower acoustic level. Such numerical methods employed in the jet aeroacoustics are not satisfactory in terms of robustness and computational cost. Grid generation around the launch-pad with complex configurations is another important issue, because such numerical method often requires "very" smooth mesh. While, the acoustic level measured in typical launchers exceeds 140dB (OASPL), which indicates that the dominant acoustic wave originates in the large-scale motion of the turbulent shear-layer. Therefore, we apply implicit LES methodology, and the jet shear-layer is computed without any turbulence model. Detail of the numerical procedures and grid system are given in the reference.[12] The Kirchhoff method is employed to calculate the sound propagation to the far-field for reducing the computational cost. Grid convergence was checked, but only one of the cases with 9.5 million nodes is discussed here. Maximum grid spacing at the acoustic propagation region inside the Kirchhoff integral surface is 0.05De. Since the present numerical scheme requires approximately 20 grid points to resolve propagating wave, the cut-off frequency in the present study is St=0.05. While, power spectrum density (PSD) of axial velocity component at the fluctuating shear layer is shown in Fig.3. The PSD decays with the slope of -5/3 until St=fUe/De=0.2, which means the turbulent structure inside the shear layer can be resolved up to this frequency. It is observed from the measurement data discussed later in Fig.7 that the peak SPL appears at around St=0.2 or lower, depending on the microphone location. Therefore, this study simulate the turbulent structure sufficiently, although the cut-off frequency results in St=0.05De.

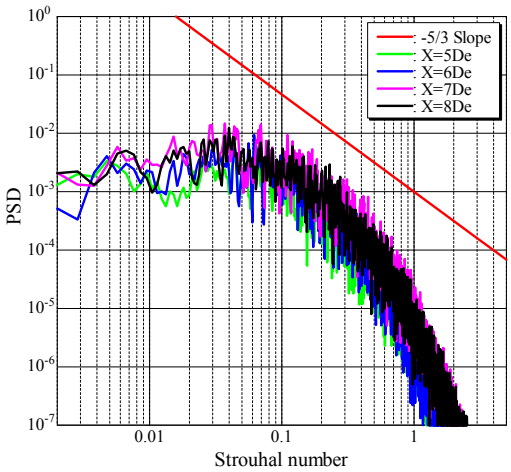

Figure 3: PSD of axial velocity at four locations indicated as the red-colored points in Fig.4.

4. Results and Discussions

4.1 Numerical Result and Validation with the Measurement Data

Time-averaged non-dimensional velocity is shown in Fig.4. Since the jet from the current motor is in the overexpanded condition as shown in Table.1, oblique shock wave emanates from the nozzle lip. Then, Mach disk is formed at X/De=0.7 where the oblique shock interacts with each other at the nozzle centerline. Divergence of velocity contour-surface is shown in Fig.5. Vorticity contour-line is also overwritten in the figure. It is observed from Fig.5 that the acoustic wave is generated and propagates obliquely downstream. The instantaneous vorticity contour-line also indicates that the slip line appearing behind the Mach disk shows unsteady

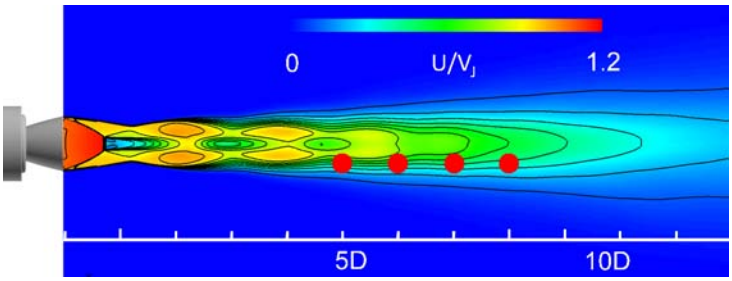

Figure 4: Distribution of time-averaged axial velocity.

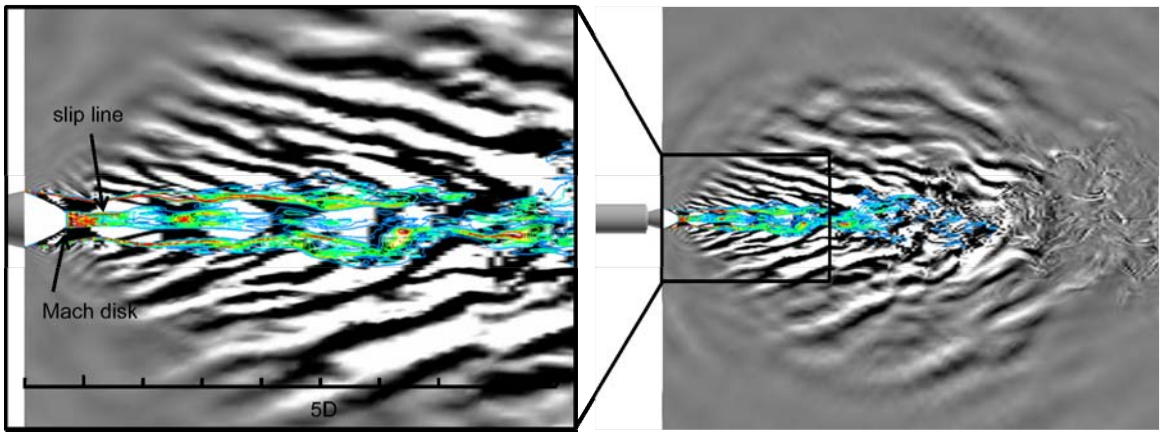

Figure 5: Divergence of velocity vector plot with vorticity contour-line.

motion. Besides, the fluctuation of the jet shear-layer is initiated at around X/De=2.0. Unsteady motion of the slip line and the jet shear-layer produces large-scale structures. Since the large-scale structures propagate downstream at the supersonic speed, the Mach wave is generated and radiated obliquely downstream as observed from the divergence of velocity shown in Fig.5. From Fig.6, Turbulent Kinetic Energy (TKE) is found to increase

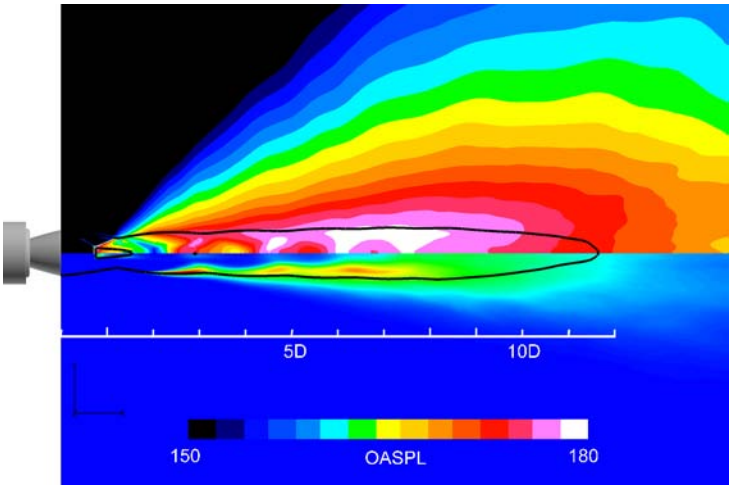

Figure 6: Distribution of OASPL (upper) and TKE (lower).

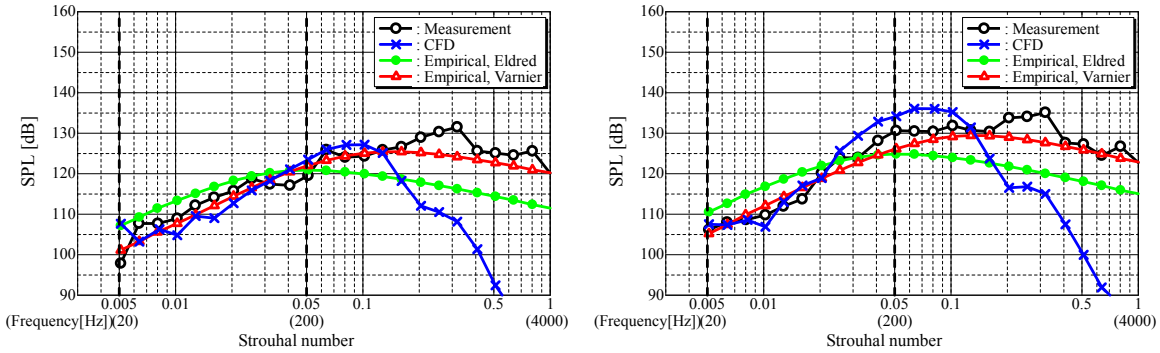

(a) M1 point (b) M2 point

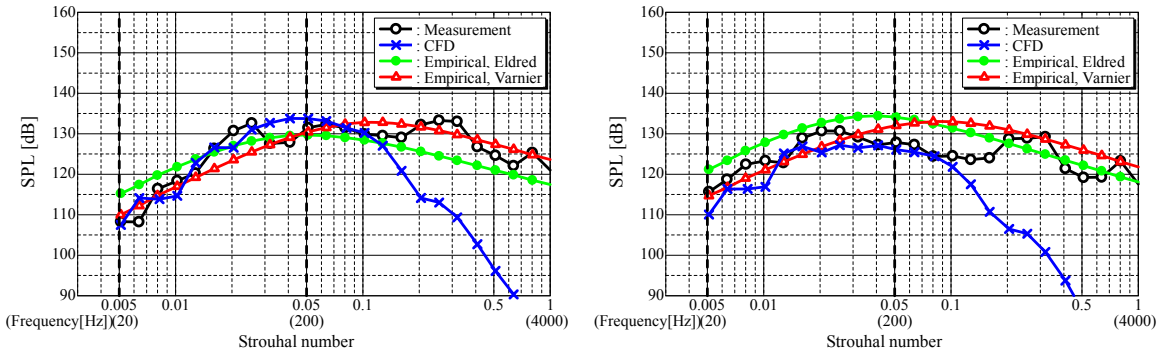

(c) M3 point (d) M4 point

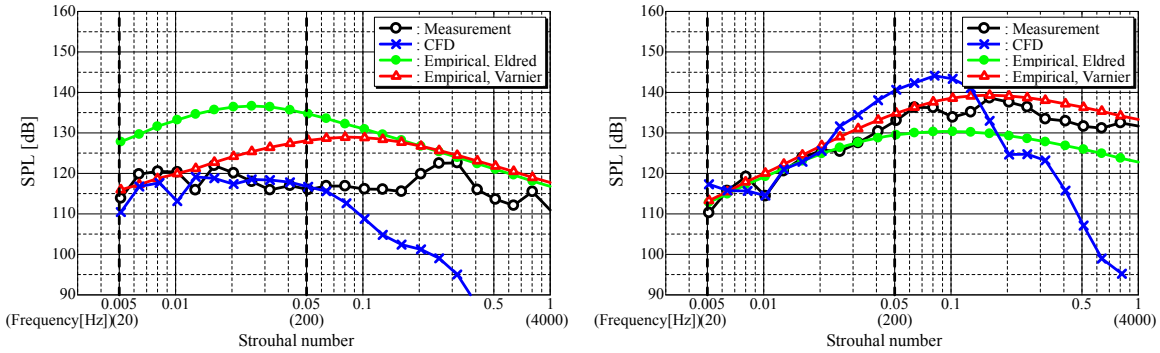

(e) M5 point (f) M6 point

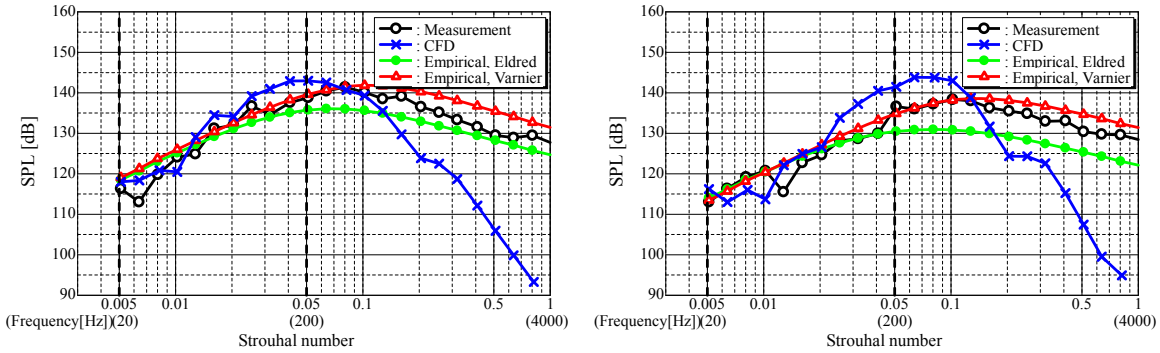

(g) M7 point (h) M8 point

Figure 7: Comparison of 1/3 octaveband SPLs.

at the region where the supersonic jet shear-layer shows unsteadiness. Distribution of over-all sound pressure level (OASPL) also indicated in the Fig.6 reveals that the dominant noise source appears at 6De-8De, which roughly corresponds to the higher TKE region.

One of the purposes in this study is to validate the prediction accuracy of the numerical method by using the measured acoustic data. Comparison of 1/3 octave-band SPLs is performed at the eight microphones in Fig.7. The location of the microphones is described in Fig.1. Though the resolved frequency range is limited in the numerical simulation (0.005<St<0.05), numerical results at the far-field microphones (M1-M5) agree well with the actual measurement. Maximum difference appears at M2 around St=0.05, but the difference is within the 5 dB at the most. Comparing with the near-field results at M6-8, the maximum difference appears at M6 and M8 around St=0.05, but the agreement is satisfactory. The OASPL at the far-field microphones is compared in Fig.8. It is found that prediction accuracy of the CFD is found to be within 4 dB in OASPL, which is satisfactory for the aim of this study.

4.2 Discussion on the Acoustic Field

It is observed from measured 1/3 octave-band SPLs colored black in Fig.7 that the peak SPL at M1 and M2 appears at St=0.05-0.1, while the peak at M4 and M5 is located at around St=0.02. These results indicate that the peak SPL shifts to the lower frequency as the microphone location close to the jet axis. In the

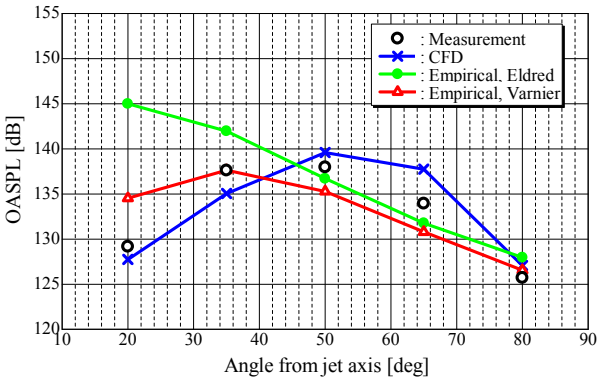

Figure 8: Comparison of OASPL (0.005<St<0.05).

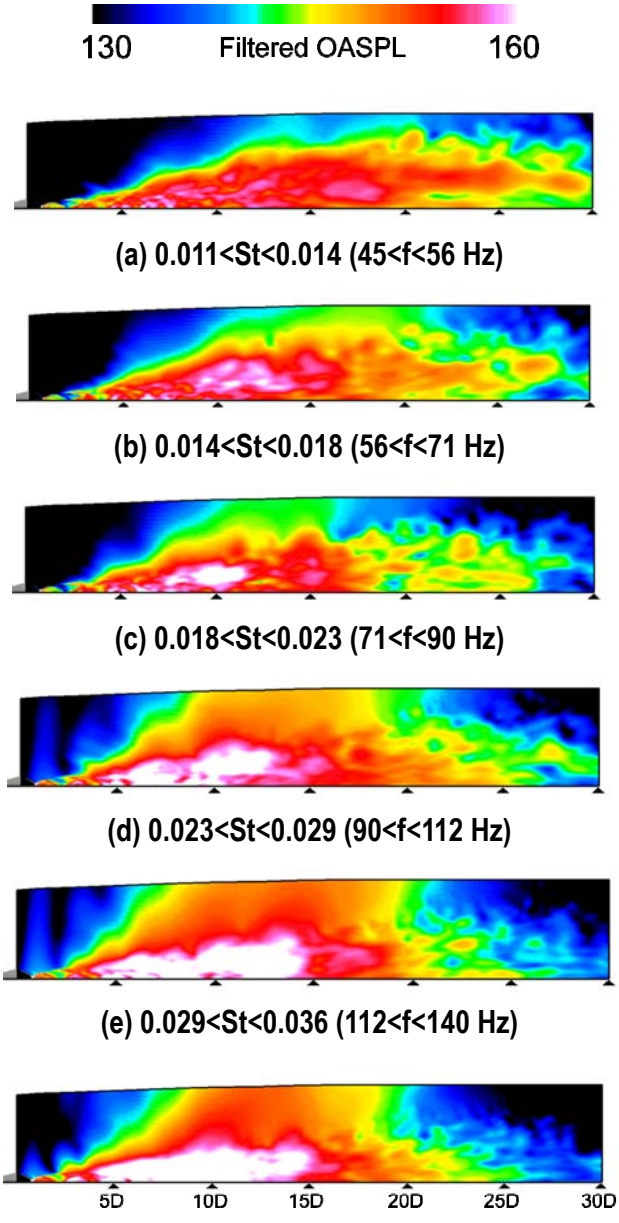

(a) 0.011<St<0.014 (45<f<56 Hz)

(b) 0.014<St<0.018 (56<f<71 Hz)

(c) 0.018<St<0.023 (71<f<90 Hz)

(d) 0.023<St<0.029 (90<f<112 Hz)

(e) 0.029<St<0.036 (112<f<140 Hz)

(f) 0.036<St<0.046 (140<f<180 Hz)

Figure 9: 1/3 octaveband filtered OASPL. Upper half from the nozlze centerline is only shown.

near-field results (M6-8), however, the peaks appear at around St=0.05-0.1. The feature observed in the near-field microphones is similar to the upstream located far-field microphones, such as M1, and M2.

In order to analyze the physical mechanism of the feature observed in Fig.7, numerical result of 1/3 octave-band filtered OASPL is shown in Fig.9. It is found from the results of Fig.9(d)-(f) (St>0.023) that strong directional feature of the Mach wave appears at 50 deg from the jet axis. The microphones of M1-M3, and M6-M8 are located upstream region of the jet, so that the directional feature observed in Fig.9 leads to the peak at the higher frequency. On the other hand, Fig.9(a) and (b) indicate the widespread distribution of the lower frequency wave. Due to the feature observed here, those microphones located downstream part of the jet, such as M4 and M5, indicate the peak of the SPLs at lower frequency than the others.

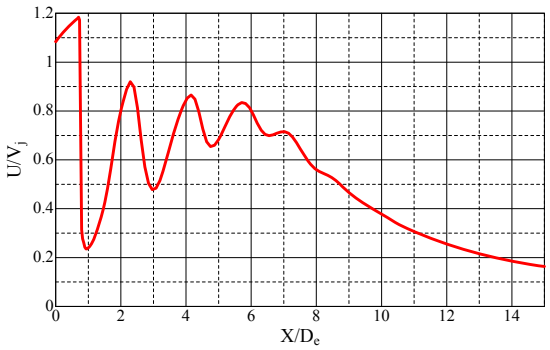

Figure 10: Axial velocity distribution of the numerical result corresponding to Fig.4.

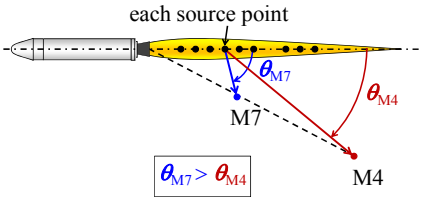

Fig.11 Schematic image of source and receiver point.

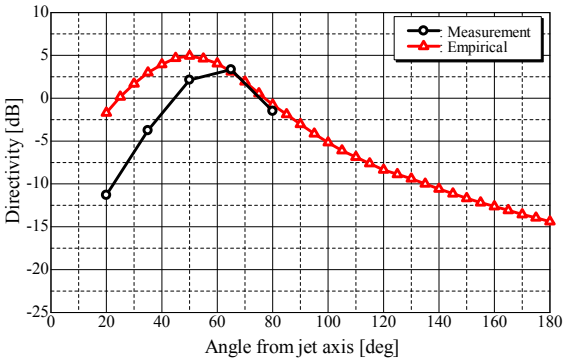

Fig.12 Comparison of directivity index at St=0.128 (f=500Hz).

4.3 Comparison of the Empirical Methods

1/3 octave-band SPLs analyzed by the empirical method can be seen in Figs.7 and 8. In these figures, predicted results based on the Eldred's model (Eq.3) and the Varnier's model (Eq.4) are indicated as green and red lines, respectively. The comparison between the analyzed SPLs and the measured values in Fig.7 (a)-(c) (M1-M3) indicates that the empirical prediction based on the Varnier's model reasonably agrees well with the actual measurement. While, in the Eldred's model, the peak frequency shifts to the lower range and the prediction error is larger. The same feature is also obtained in the comparison of the near-field microphones (M6-M8). Based on the results of M1-M3 and M6-M8, the acoustic efficiency estimated from Eqs. 1 and 2 is found to be reasonable. On the other hand, both the Eldred's and Varnier's models overestimate the SPL at M4, M5 (Fig.7 (d), (e)). Difference more than 10 dB at St=0.05-0.16 is observed in the result of M5. The OASPL distribution compared in Fig.8 indicates that the directional feature analyzed by the Varnier's model is roughly at 35 deg, which is lower than the measured value and the numerical result. No noticeable peak is found in the Eldred's model. The overestimation at M4 and M5 (Fig.7 (d), (e)) is related to the discrepancy appearing in the OASPL.

In order to find out the reason for the overestimation observed in the empirical predictions, the models of the potential-core length and the directivity are discussed. As mentioned in the section 2.1, the model of the potential-core length is sensitive to the result because it defines the source-power distribution along the jet axis. Numerical result of the axial-velocity distribution along the jet axis is indicated in Fig. 10, which indicates that the potential-core length (Lc) in the numerical simulation is roughly 7De. On the other hand, Lc evaluated by the Eldred's and Varnier's models is 15.4De and 4.8De, respectively. The Varnier's model is close to the numerical result, while the length estimated by the Eldred's is around 3 times longer. According to Fig.2, the sound-power peak location (Lp) is about 1.5Lc. In the Varnier's model, Lp is evaluated as 8.7De. In the numerical result shown in Fig.6, peak of the OASPL is located around 6De-8De, which agrees well with the analyzed location based on the Varnier's model, although ratio of Lp to Lc in the numerical simulation corresponds to 0.85-1.14. On the other hand, Lp is computed to 23.1De in the Eldred's model, which is too long. The discussion here supports the recent studies that the Varnier's model is appropriate. [4,6,7]

Even if the Varner's model reasonably predicts the sound-power peak location, discrepancy still exists in the microphones of M4 and M5. Further discussion on the directivity model is performed to analyze the reason for the overestimation. Two microphones of M4 and M7 are focused firstly. Note that the empirical prediction method overestimates the SPL at the M4, but reasonably estimates the SPL at the M7. It is observed from Fig.11 that these two points are located at roughly the same angle (35 deg) from the nozzle exit. However, in the empirical method, the angle used for the directivity model is from the point source located at each slice of the jet. Considering the angle from the peak-source location of the Varnier's model at X=8.7De for example, the angles to M4 (θ_{M4}) and to M7 (θ_{M7}) are 40.4 deg and 52.5 deg, respectively. Therefore, it is deduced that the directivity model for the small angle is inappropriate. In Fig.12, directivity index evaluated from the actual measurement based on Eq.5 are compared with the NASA SP-8072 model at St=0.128 (f=500 Hz). The directivity index of the NASA SP-8072 at 40.4 deg is about 11 dB higher than that of the measurement, but the difference between them at 52.5 deg decreases to be 3 dB. This is the reason why the analyzed SPL at M4 overestimates more than 10 dB regardless of the potential-core length models.

5. Concluding Remarks

In order to predict the acoustics level due to the rocket plume, numerical simulation and the empirical prediction method were investigated by using the results of the static-firing tests of a solid motor. It turns out from the numerical study using the implicit LES that the fluctuating supersonic jet shear-layer generates the Mach wave. The numerical simulation can reasonably predict SPLs at all measurement points including both of the near- and the far-field. Prediction accuracy is found to be within 4 dB in OASPL.

In the study of the empirical method, two models for the potential-core length are compared. It turns out that the potential-core length based on the Varnier's model is close to the numerical result, while the NASA

SP-8072's model is 3 times longer. Besides, the Varnier's model is revealed to be effective for the far-field prediction, but there is still notable discrepancy at the microphones close to the jet axis. The directvity index described in the NASA SP-8072 is compared with the computed directivity index from the measurement. It is revealed that the directivity index based on the NASA SP-8072 is much higher at smaller angle, which leads to the discrepancy observed in this study. Effect of the directivity model is found to be considerable in the empirical prediction.

References

[1] Eldred,K.M., and et al., "Acoustic Loads Generated by the Propulsion System," NASA SP-8072, June, 1971.

[2] Koudriavtsev, V. V., "Acoustic Model for Supersonic Jet Interaction with a Complex Deflector", Proceedings of The 6th European Symposium on Aerothermodynamics for Space Vehicles, Nov., 2008.

[3] Dumnov, G., Mel'nikov, G., and Komarov, V., "Acoustics Loads on Rockets During Launching", AIAA 2000-3742, July, 2000

[4] Varnier, J., "Experimental Study and Simulation of Rocket Engine Freejet Noise," *AIAA Journal*, Vol. 39, No. 10, Oct. 2001, pp. 1851-1859.

[5] Casalino, D., Barbarino, M., Genito, M., and Ferrara, V., " Improved Empirical Methods for Rocket Noise Prediction through CAA Computation of Elementary Source Fields," AIAA 2008-2939, May 2008.

[6] Haynes, J., Kenny, R. J., "Modification to the NASA SP-8072 Distributed Source Method II for Ares I Lift-off Environment Predictions", AIAA 2009-3160, May, 2009.

[7] Plotkin, K. J., Sutherland, L. C., and Vu, B. T., "Lift-off Acoustics Predictions for the Ares I Launch Pad", AIAA 2009-3163, May, 2009.

[8] Sutherland, L. C., "Progress and Problems in Rocket Noise Prediction for Ground Facilities", AIAA 93-4383, Oct., 1993.

[9] Tsutsumi, S., Takaki, R., Shima, E., Fujii, K., and Arita, M., "Generation and Propagation of Pressure waves from H-IIA Launch Vehicle at Lift-off", AIAA 2008-390, Jan.2008.

[10] Tsutsumi, S., Fukuda, K., Takaki, R., Shima, E., Fujii, K., and Ui, K., "Numerical Study on Acoustic Radiation for Designing Launch-Pad of Advanced Solid Rocket," AIAA 2008-5148, July 2008.

[11] Tsutsumi, S., Kato, S., Fukuda, K., Takaki, R., and Ui, K., "Effect of Deflector Shape on Ascoutic Field of Launch Vehicle at lift-off," AIAA 2009-328, Jan., 2009.

[12] Fukuda, K., Tsutsumi, S., Fujii, K., Ui, K., Ishii, T, Oinuma, H., Kazawa, J., and Minusugi, K., "Acoustic Measurement and Prediction of Solid Rockets in Static Firing Tests", AIAA 2009-3368, May, 2009.

[13] Horne, W. C., Burnside, N. J., Panda, J., and Brodell, C., "Measurements of Unsteady Pressures near the Plume of a Solid Rocket Motor", AIAA 2009-3323, May, 2009.

[14] Bodony, D. J., and Lele, S. K., "Review of the Current Status of Jet Noise Prediction Using Large-Eddy Simulation", AIAA 2006-136, Jan., 2006.